

JGR Space Physics

















RESEARCH ARTICLE

10.1029/2020JA028052

Special Section:

Jupiter Midway Through the Juno Mission

Heavy Ion Charge States in Jupiter's Polar Magnetosphere Inferred From Auroral Megavolt Electric Potentials

G. Clark¹ , B. H. Mauk¹ , P. Kollmann¹ , C. Paranicas¹ , F. Bagenal² , R. C. Allen¹ , S. Bingham¹ , S. Bolton³ , I. Cohen¹ , R. W. Ebert^{3,4} , W. Dunn⁵ , D. Haggerty¹ , S. J. Houston¹, C. M. Jackman^{6,7} , E. Roussos⁸ , A. Rymer¹ , and J. H. Westlake¹ 

Key Points:

- Quasi-static electric potentials in Jupiter's polar cap region are used to determine the energetic (>hundreds of keV) ion charge states
- The most abundant charge states associated with these precipitating ions are O^+ and S^{++} and therefore iogenic in origin
- These observations are important for X-ray auroral and ion-neutral interaction physics

Correspondence to:

G. Clark,
george.clark@jhuapl.edu

Citation:

Clark, G., Mauk, B. H., Kollmann, P., Paranicas, C., Bagenal, F., Allen, R. C., et al. (2020). Heavy ion charge states in Jupiter's polar magnetosphere inferred from auroral megavolt electric potentials. *Journal of Geophysical Research: Space Physics*, 125, e2020JA028052. <https://doi.org/10.1029/2020JA028052>

Received 26 MAR 2020

Accepted 16 JUN 2020

Accepted article online 16 JUL 2020

¹Johns Hopkins University Applied Physics Laboratory, Laurel, MD, USA, ²Laboratory for Atmospheric and Space Physics, University of Colorado Boulder, Boulder, CO, USA, ³Southwest Research Institute, San Antonio, TX, USA, ⁴Department of Physics and Astronomy, University of Texas at San Antonio, San Antonio, TX, USA, ⁵Mullard Space Science Laboratory, Department of Space and Climate Physics, University of College London, London, UK, ⁶School of Physics and Astronomy, University of Southampton, Southampton, UK, ⁷Astronomy and Astrophysics Section, Dublin Institute for Advanced Studies, Dublin, Ireland, ⁸Max Planck Institute for Solar System Research, Göttingen, Germany

Abstract In this paper, we exploit the charge-dependent nature of auroral phenomena in Jupiter's polar cap region to infer the charge states of energetic oxygen and sulfur. To date, there are very limited and sparse measurements of the >50 keV oxygen and sulfur charge states, yet many studies have demonstrated their importance in understanding the details of various physical processes, such as X-ray aurora, ion-neutral interactions in Jupiter's neutral cloud, and particle acceleration theories. In this contribution, we develop a technique to determine the most abundant charge states associated with heavy ions in Jupiter's polar magnetosphere. We find that O^+ and S^{++} are the most abundant and therefore iogenic in origin. The results are important because they provide (1) strong evidence that soft X-ray sources are likely due to charge stripping of magnetospheric ions and (2) a more complete spatial map of the oxygen and sulfur charge states, which is important for understanding how the charge- and mass-dependent physical processes sculpt the energetic particles throughout the Jovian magnetosphere.

1. Introduction

Neutral gases are continuously liberated from the surfaces and atmospheres of the Galilean moons and are the source of heavy ions in Jupiter's magnetosphere. The dominant neutral source is from Io and likely through the form of sulfur dioxide (SO_2), which rapidly dissociates into S and O (e.g., reviews by Bagenal & Dols, 2020; Schneider & Bagenal, 2007; Thomas et al., 2004). To a lesser, and still poorly understood, extent, the other Galilean moons, Europa, Ganymede, and Callisto, also serve as neutral sources (e.g., Hansen et al., 2005, and review by Kivelson et al., 2004). Some fraction of these neutrals is ionized via photoionization, electron impact ionization, and charge exchange. These freshly created ions are then entrained in the local plasma flow and are subject to the electromagnetic forces, which accelerate them to the local corotational energy. As the heavy ions spread out, they create a large, extended structure confined near the magnetic equator and play a crucial role in nearly all aspects of the formation, structure, and dynamics of Jupiter's space environment (e.g., reviews by Khurana et al., 2004; Krupp et al., 2004). Therefore, understanding the sources, sinks, and transport of these heavy ions is crucial to understanding Jupiter's plasma and energetic charged particle environment. These processes are usually inferred through specific measurements of the ion population. One such measurement is the charge state distribution of the heavy ions. Charge states can provide physical insight into the following processes: ion-neutral interactions in Jupiter's neutral cloud (e.g., Clark et al., 2016; Kollmann et al., 2016; Lagg et al., 2003; Mauk et al., 2004; N n n & Andr e, 2019; Paranicas et al., 2009), ion escape across the magnetopause (Mauk et al., 2019) and solar wind entry (e.g., Allen et al., 2018, 2019), physical ion-chemistry taking place in the vicinity of Io and Europa (e.g., Bagenal & Delamere, 2011; Delamere et al., 2007; Smith et al., 2019), acceleration mechanisms (e.g., Kronberg et al., 2019), and sources of X-ray emissions in Jupiter's polar auroral regions (e.g., Branduardi-Raymont et al., 2007; Cravens et al., 2003; Dunn et al., 2017; Houston et al., 2018; Jackman et al., 2018; Ozak et al., 2010).

It is important to distinguish the differences between lower-energy plasma and higher-energy energetic charged particles. It is an imprecise demarcation, but charged particles start strongly separating from one another due to gradient-curvature drifts in Jupiter's inner magnetosphere above about 1 keV. Energetic charged particles have densities much lower than the cold plasma, but their energy density and higher-order moments, that is, pressure, can be significant and their contribution to the magnetosphere cannot be ignored—this is especially true for Jupiter (e.g., Mauk et al., 2004). Historically, different measurement techniques have been applied to the two populations. For energetic particles, the solid-state detector and coincidence technique is not suited for charge state separations. These two populations are typically measured using different techniques, in which the mass-per-charge is measured for the thermal plasma, while for energetic particles, the mass is accurately known without a charge dependence. This has resulted in most charge state studies to be limited to only the thermal energy range. In fact, the charge states for the energetic population at Jupiter, with the exception of one case study (Allen et al., 2019), have been inferred via charge state dependent plasma processes, that is, gradient-curvature drifts (Clark, Mauk, et al., 2016) or moon microsignatures (Selesnick & Cohen, 2009). Furthermore, measurements have been limited to a general region of Jupiter's inner-to-middle equatorial magnetosphere. This is largely due to the nature of using the phenomenological changes in the ion distributions near the moons or Jupiter's neutral cloud to infer the bulk charge state.

Clark, Mauk, et al. (2016) analyzed several injection events using the Galileo Energetic Particle Detector and found that energetic ion (~ 0.3 to 5 MeV) charge states are predominately multiply charged for sulfur (S^{++} most probable) and more evenly distributed between O^+ and O^{++} for oxygen. Compared to the lower-energy plasma, these observations suggested higher proportions of O^{++} . Clark, Mauk, et al. (2016) hypothesized that at energies greater than hundreds of keV, the charge stripping cross sections become important and the neutral cloud in the vicinity of Europa may be redistributing the oxygen charge states to higher proportions of O^{++} . This conclusion was also used to further support the idea of a trans-Europa gas cloud and its species-dependent interactions with the energetic ions originally proposed by Lagg et al. (2003) and Mauk et al. (2003). Nénon and André (2019) also provided circumstantial evidence for multiply charged sulfur ions by inspecting their losses near Europa.

A recent analysis of the Cassini energetic particle data during its Jupiter flyby is the only direct measurement to date of the >50 keV/q heavy ion charge state distributions (Allen et al., 2019). Unfortunately, Cassini only entered Jupiter's magnetosphere briefly on the dusk side (~ 200 Jovian radii (R_J)), and the Charge-Energy-Mass Spectrometer had its electrostatic analyzer voltage fixed, so only ~ 100 keV/q ions were measured, for ~ 1 hr. Despite these limitations, Allen et al. (2019) found the charge state distributions near the magnetopause are consistent with the plasma measurements in the inner magnetosphere and attributed any differences to energy or charge-dependent heating and/or energization mechanisms.

At much higher energies (≥ 5 MeV/nucleon), the charge states of oxygen and sulfur appear to have a larger uncertainty. Garrard et al. (1996) analyzed the Galileo Heavy Ion Counter (HIC) data and found the compositional ratios in the vicinity of Io to best match singly charged oxygen and sulfur. Their conclusion was based on the weak absorption signatures observed near Io, and they postulated that ions with higher charge states would have increased absorption due to smaller gyroradii. Similarly, Cohen et al. (2001) found evidence for singly charged oxygen and sulfur near $10 R_J$ by analyzing abundance ratios measured by HIC. In contrast to these two previous results, Selesnick and Cohen (2009) found the very energetic ion charge states to be fully, or almost fully, stripped in the vicinity of Io. This conclusion is based on numerical simulations of microsignatures (including the effect of Io's Alfvén wing) to explain ion depletions observed by Galileo's HIC in Jupiter's radiation belt. Additional evidence for high charge state heavy ions comes from soft X-ray emissions near Io, Europa, and the Io Plasma Torus (Elsner et al., 2002). However, Elsner et al. (2002) could not reconcile the soft X-ray intensities with high charge state oxygen alone and suggested bremsstrahlung emission from the nonthermal electrons may be playing a key role.

In this contribution, we provide new experimental results of the oxygen and sulfur charges states in Jupiter's polar magnetosphere from NASA's Juno mission (Bagenal et al., 2017; Bolton et al., 2017; Connerney, Adriani et al., 2017). Similar to previous techniques, the method in this paper relies on circumstantial evidence and exploits the charge-dependent acceleration mechanisms in Jupiter's polar cap auroral region, specifically, the quasi-static megavolt electric potentials that were discovered by Clark et al. (2017). This study

adds to the subject regarding how charge states are distributed in Jupiter's magnetosphere, and we discuss the implications of our results in the context of previous work regarding ion-neutral interactions and Jupiter's X-ray aurorae.

2. Juno/JEDI Instrument Data Selection and Reduction

Ion observations presented in this study were obtained from the Jupiter Energetic particle Detector Instrument (JEDI), which is onboard NASA's Juno spacecraft—a Jupiter polar orbiting mission. JEDI comprises three sensors which are commonly referred to as JEDI-90, JEDI-180, and JEDI-270 (or simply J180, etc.; Mauk et al., 2017). The J90 and J270 sensors utilize a time-of-flight and solid-state detector energy system to measure the velocity and total energy of the incident ions greater than ~50 keV for protons, greater than ~400 keV for separation of oxygen and sulfur. At lower energies, JEDI cannot distinguish between O and S; however, it can measure their combined energy and angular distributions. Sensors J90 and J270 are configured on the spacecraft deck such that their fields of view (FoV) are nearly in the spin plane of Juno. This orientation was chosen to optimize the angular coverage of the magnetic field-aligned particles over Jupiter's auroral regions, but it has the limitation of not sweeping out the full sky (4π solid angle).

The ion measurements in this paper were collected when JEDI was in a high-energy-resolution and high-rate mode, thus collecting data at a cadence of 0.5 s without sector averaging. This is the typical mode of operation of the JEDI instruments suite when Juno passes over Jupiter's polar regions. The nature of Juno's orbit is that it passes over the polar cap and main auroral regions at relatively low altitudes (often below $2 R_J$ but sometimes as close as $\sim 1/3 R_J$), translating to a local geometric loss cone $>10^\circ$. This is important because the heavy ions studied are precipitating into Jupiter's atmosphere; due to JEDI's FoV is approximately $12^\circ \times 18^\circ$ FoV, JEDI can often resolve the loss cone.

Although the data are collected at a fairly high cadence, time-averaging windows on the order of ~10 s are often used to increase the total counts in any given energy channel. Additionally, since the ion distributions measured are highly directional and aligned with the local magnetic field, pitch angle filtering is employed to capture the features of interest, that is, those within the loss cone. Unless otherwise noted, the pitch angles were filtered to $\pm 30^\circ$ of the field-aligned direction and calculated using the Juno Magnetometer calibrated data set (Connerney, Bann et al., 2017).

We use the method outlined in Mauk et al. (2004, see Equation 2) to calculate the partial densities of energetic O^{n+} and S^{n+} , where n represents all possible integer charge states for the given ion. The partial number density equation is given as follows: $N(\text{cm}^{-3}) = 4\pi \sqrt{\frac{1}{2m}} \int \frac{I}{E} \sqrt{E} dE$, where I is the differential intensity in $\text{cm}^{-2} \text{s}^{-1} \text{sr}^{-1} \text{erg}^{-1}$, m is the ion mass in grams (g), and E is the energy in erg. The equation assumes angular isotropy, which we know is not true for these observations; however, since we are interested in the ratio of the heavy ion densities, we believe this formalism still provides useful information even if the absolute values are not accurate.

3. Inference Technique: Charge-Dependent Acceleration in Megavolt Electric Potentials

NASA's Juno mission revealed the presence of large-scale electric potentials embedded within Jupiter's polar cap region (Clark et al., 2017). These quasi-static, electric potentials were discovered by energetic ion and electron signatures. In this region, the precipitating ions were aligned with the local magnetic field and exhibited sharp peaks, which resembled accelerated Maxwellian distributions, in phase space density. Adjacent in time/space, electrons were moving antiplanetward along the magnetic field and also had sharp peaks in phase space density. The peak energies associated with the ions and electrons were ~1 MeV and ~400 keV, respectively. Although Juno does not have a DC electric field experiment, we understand these type of particle distributions to be consistent with acceleration via magnetic field-aligned electric fields as observed at Earth (e.g., Ergun et al., 1998). Additionally, the ion and electron measurements from Juno clearly resemble the canonical "inverted-V" type distribution that is often observed in Earth's main auroral region (e.g., Carlson et al., 1998; Lin & Hoffman, 1982). Subsequent studies of the large-scale megavolt potentials reveal that they are often embedded in Jupiter's polar cap region and span all System III

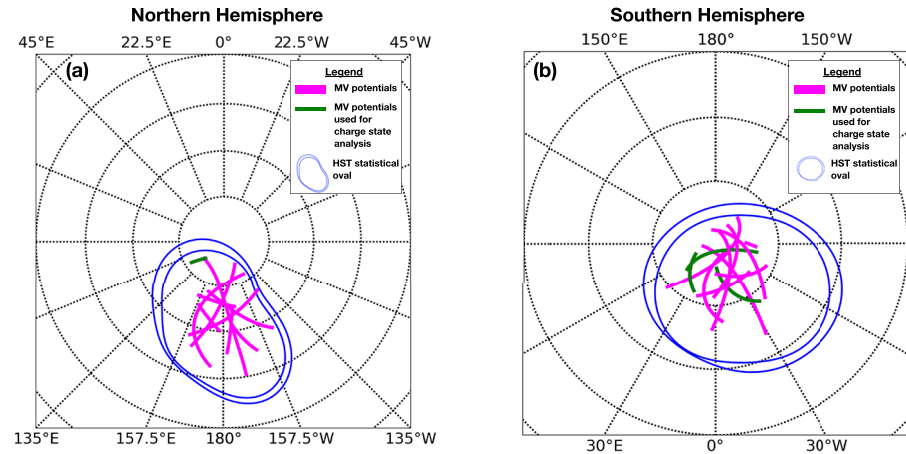


Figure 1. System III longitude and latitude locations of observed megavolt electric potentials from Juno/JEDI spanning Perijoves 1–16. (a) Northern hemisphere projection of the Hubble Space Telescope (HST) statistical main auroral oval (blue curves) and the locations of the MV potentials mapped along the Jupiter’s magnetic field to ~400 km above the 1 bar surface using the JRM09 magnetic field model (Connerney et al., 2018) and the magnetodisc model from Connerney et al. (1981). (b) Similar to (a) except for the southern hemispheric projection.

longitudes and latitudes poleward of Jupiter’s main oval (Mauk et al., 2020). Figure 1 depicts the locations of the observed MV potential structures studied by Mauk et al. (2020) in a Jupiter System III coordinate system (magenta curves) and the MV potential observations used for our charge state analysis (green curves). The reasons only a subset of observations is chosen for this study is discussed later in this section.

Clark et al. (2017) used Juno/JEDI measurements of the protons and heavy ions, that is, oxygen and sulfur, within a single event to infer the heavy ions were magnetospheric in origin. This was achieved by comparing the peak energies between the various ions and assuming that quasi-static, parallel electric fields accelerated the ions proportional to their charge state. In other words, $E = q\Phi$, where E is the potential energy, q is the ion’s charge, and Φ is the electric potential strength. Protons were used as the fiducial since their charge state is equal to one. Differences in the peak energies between the oxygen and sulfur ions were purely due to their corresponding charge states. The single case study suggested the oxygen and sulfur ions were low-charge state and therefore magnetospheric in origin. This is the basis of the technique used here; however, we further develop the approach and apply it to several Juno perijove (PJ) orbits.

In Figure 2, we show the proton (Figure 2a), oxygen (Figure 2b), sulfur (Figure 2c), and combined oxygen and sulfur energy channels (Figure 2d) that clearly show an example of a quasi-static, MV electric potential. From approximately 08:55 to 09:03 UT on Year 2018, Day of Year 091 (PJ12), the Juno/JEDI > 50 keV proton measurements show peaked energy distributions that increase with time at first, plateau, and then decrease, thus, creating the so-called “inverted-V” pattern. The plateau energy that occurs near the apex of the “V” is ~1 MeV. In the following panels (Figures 2b–2d), the heavy ions also resemble a similar profile. However, due to the selection of JEDI’s science priorities, these channels are much broader in energy and depict a less clear inverted-V profile. JEDI does not have the ability to discern oxygen from sulfur at energies ≤ 350 keV. Therefore, JEDI combines these oxygen and sulfur events into “heavy ion” channels, which extends the heavy ion measurements down to ~170 keV (Figure 2d). Note, we include these channels in our analysis and discuss the implications in the next section.

Overlaid in each panel of Figure 2 is a red curve corresponding to the peak energy at a given time corresponding to the characteristic energy, $\langle E \rangle$, of the ion distribution. We calculate $\langle E \rangle$ using the same formula as Clark et al. (2018) and Mauk et al. (2004), which used it to study Jupiter’s auroral acceleration mechanisms and hot plasma parameters in the equatorial magnetosphere, respectively. The equation is $\langle E \rangle = \frac{\sum_i I_i E_i \Delta E_i}{\sum_i I_i \Delta E_i}$, where E_i is the centroid energy, ΔE_i is the energy width, and I_i is the particle intensity measured at a given energy channel i , where i ranges from ~50 keV to 2.5 MeV for protons, ~400 keV to 6 MeV for oxygen, and ~600 keV to 7 MeV for sulfur. The characteristic energy can also be thought as an energy-weighted sum of the differential intensity spectrum. It was found that for auroral

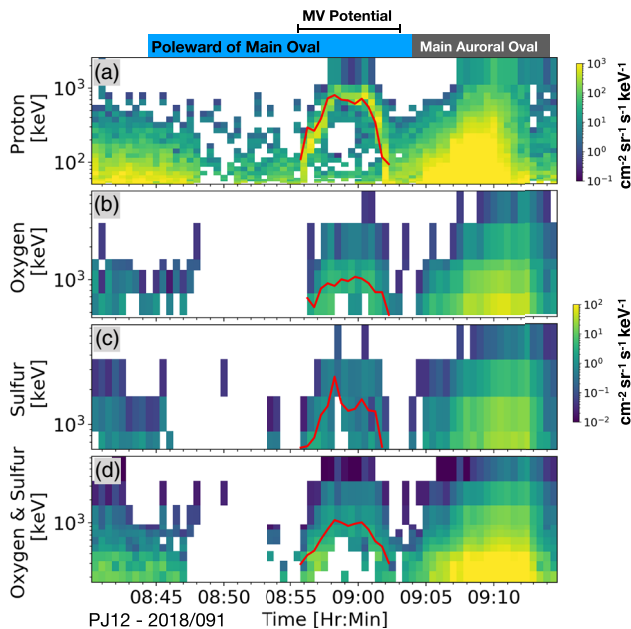


Figure 2. Proton (a), oxygen (b), sulfur (c), and combined oxygen and sulfur (d) energy-time spectrograms. Pixels are coded by their differential intensity corresponding to the color bars. (b)–(d) share a common color bar. The red curve corresponds to the calculated characteristic energy and is used to retrieve associated proton and heavy ion peak energies (see text).

technique, we find the most abundant charge states and scatter intervals to be 1.37 ± 1.51 for oxygen and 1.96 ± 1.19 for sulfur. It is known from plasma measurements (e.g., Allen et al., 2019; Bagenal et al., 2017; Kim et al., 2020) that multiply charged oxygen exists, albeit at lower abundances. In fact, the ratio being slightly larger than 1 for oxygen likely implies that the accelerated distribution contains an admixture of charge states; however, JEDI is not sensitive enough to measure them individually. This result merely provides a proof of concept for the method and note that the fits do a much better job representing the charge state distributions when we consider multiple perijoves, as we do in the next section.

Finally, in Appendix A, we layout another method to infer the oxygen and sulfur charge states from Juno/JEDI measurements. The method in Appendix A relies on an ion energy correlation technique that was first developed by Mitchell et al. (2018) to explore the charge-dependent adiabatic energization of ions in Earth’s magnetosphere. The results validate the method above but have limited shortcomings which are discussed in Appendix A.

4. Energetic Oxygen and Sulfur Ion Charge State Results

Figure 2a is an example of a “clean” proton inverted-V profile, meaning the energy-time dependence is continuous and captured completely within the dynamic energy range of the proton channels. It is often found that the charged particle signatures associated with these MV potentials are not always as clear as the example in section 3. Figures 4a–4d show proton energy-time profiles within MV potentials that were used in this analysis. Figure 4e shows an example of a MV potential that exhibited intermittent intensities, which rapidly evolve toward energies beyond the instrument’s measurement capability. Furthermore, the decreasing energy portion of the inverted-V profile in Figure 4e is either nonexistent or merges into the main auroral oval and is not an ideal candidate for this type of analysis. For these reasons, we omit this event from our analysis as well as many other perijove passes. We are left with four strong observational candidates: PJ6, PJ7, PJ12, and PJ14.

In Figure 5, we show the frequency distributions associated with the characteristic energy ratios derived from the MV potentials events shown in Figures 4a–4d. The distributions resemble a log-normal shape with geometric means for oxygen at $\mu = 1.37 \pm 0.60$ and for sulfur at $\mu = 2.35 \pm 1.80$. The reported error is the

distributions, $\langle E \rangle$ can be used as a peak finder. Differences between measured energy peaks and the characteristic energy can exist and begin to deviate significantly when the gradients in intensity near the peak energy become shallow and more broadband. This is often not the case for the ion distribution in Jupiter’s polar cap region. Measurements from the Jovian Auroral Distribution Experiment-Ion sensor show there are relatively little or no heavy ions (less than or equal to ~ 40 keV/Q) poleward of Jupiter’s main auroral oval region (Szalay et al., 2017). Therefore, including the low-energy data will not impact the characteristic energies derived based on JEDI observations alone.

Ratios between proton, oxygen, and sulfur characteristic energies as a function of time across the inverted-V can be used to approximate the most abundant charge state. For example, doubly charged oxygen will be accelerated in the inverted-V to twice the energy as a singly charged proton. Following our previous discussion on the charged dependent acceleration, we attribute the differences in the total energy gained from the ions acted upon by the same potential to their charge states. Using protons as the fiducial for $q = 1$, we can infer the charge states of the heavier ions. Figure 3 shows an example histogram of the oxygen-to-proton and sulfur-to-proton characteristic energy ratios for this perijove. The log-normal density function is then used to fit the frequency distributions to obtain the geometric mean (i.e., μ , the most abundant charge state) and scatter intervals (i.e., σ). For this single event analysis, used to only illustrate the tech-

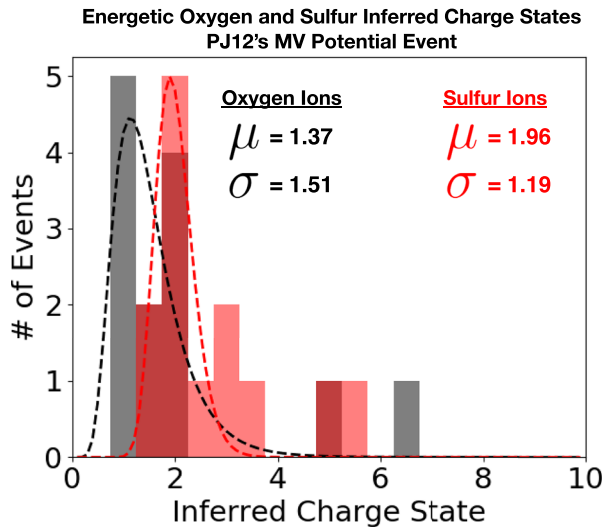


Figure 3. Frequency distributions of the oxygen and sulfur ion to proton characteristic energy ratios (which we call “inferred charge state” on the abscissa axis) for the PJ12 event shown in Figure 2. Log-normal fits to the frequency distributions reveal the geometric mean, μ , and scatter intervals, σ . Each event corresponds to a time sample within the MV inverted-V potential.

scatter interval that contains two thirds of the events from the log-normal fits (black dashed curves in Figure 5). As discussed in section 3, these values represent the most abundant charge states of the ion population falling through the electric potential. One can crudely assume a distribution of charge states and see which abundance ratio yields the peak values reported here. For example, a distribution of oxygen that has three times more O^+ than O^{++} may yield a μ of ~ 1.37 . Similarly, if S^{++} is four times more abundant than both S^+ and S^{+++} , a μ of ~ 2.35 results. In no certain terms does this act as a proof, since the observations presented here lack the ability to truly estimate the abundances. However, this crude estimate reflects the measured distributions from previous results (Allen et al., 2019). Inferred charge state values less than one can be attributed to the sometimes-small differences between the energy peak and the characteristic energy of the ion distributions (see section 3, paragraph 4).

In Figure 5c, we also show the ratio of characteristic energies between the combined O^{n+} and S^{n+} channels—effectively extending the heavy ion measurements down to ~ 170 keV total energy. In practice, since these are not species resolved channels, the interpretation of the result is limited, despite results from partial density calculations (based off the method shown in section 2) that reveal mixed species energy channels are likely dominated by oxygen ions. Figure 6

shows the frequency distributions of the O^{n+} to S^{n+} partial density calculations within the observed MV potentials (bars), and we conclude that since the mean ratio is 1.63 ± 0.53 , that O is dominant. If this holds true, this allows us to extend our claim that O^+ is the most abundant charge state down to ~ 170 keV (see Figure 5c).

After considering charge ratios, we now consider the mass ratios. Note that mass separation can be done through nominal instrument capabilities and does not require MV potential events. Here, we compare the partial density O^{n+} to S^{n+} ratios associated with the MV potentials to their counterpart in the magnetic equator. First, the MV potentials were mapped back to the magnetic equator using the JRM09 model (Connerney et al., 2018), and we found the majority of events in Figure 1 spans ~ 60 to $85 R_J$. Then we chose an arbitrary time period when Juno was near the distant magnetic equator ($60\text{--}85 R_J$) and JEDI was collecting ion data—the dates cover three days from 2017-183 to 2017-186. It is important to note that the radial distance comparisons are not perfect because magnetic mapping beyond $30 R_J$ is still unreliable, variable, and model dependent. In Figure 6, the mass ratios show that near the equator, the energetic ion population is more sulfur abundant (this also agrees with Galileo measurements presented in Mauk et al., 2004), which contrasts the more oxygen abundant ratios associated with the MV potentials. We discuss possible interpretations for this difference in the next section.

We recognize that JEDI’s energy channels for O^{n+} and S^{n+} differ slightly, so for completeness, we present two methods to derive the mass ratios: (Method 1) integrating only over the overlapping energies (see red histogram bars in Figure 6) and (Method 2) integrating over all the O^{n+} and S^{n+} energy channels (see red trace in Figure 6). We believe Method 1 is more meaningful, but we demonstrate that for reasonable choices on the energy limits, the equatorial distributions still differ from the high-latitude ones.

5. Discussion

5.1. Heavy Ion Charge States

Our analysis of the Jovian high-latitude, low-altitude polar region reveals that heavy ion charge states are predominately O^+ and S^{++} with a small contribution from O^{++} and S^+ as well as S^{+++} . This charge state imprint suggests that the majority of heavy ions in this region is iogenic in origin and agrees reasonably well with charge state abundances derived from plasma measurements in the inner-to-middle magnetosphere, that is, $\lesssim 40 R_J$ (e.g., Bagenal et al., 2017; Kim et al., 2020). Additional evidence comes from the

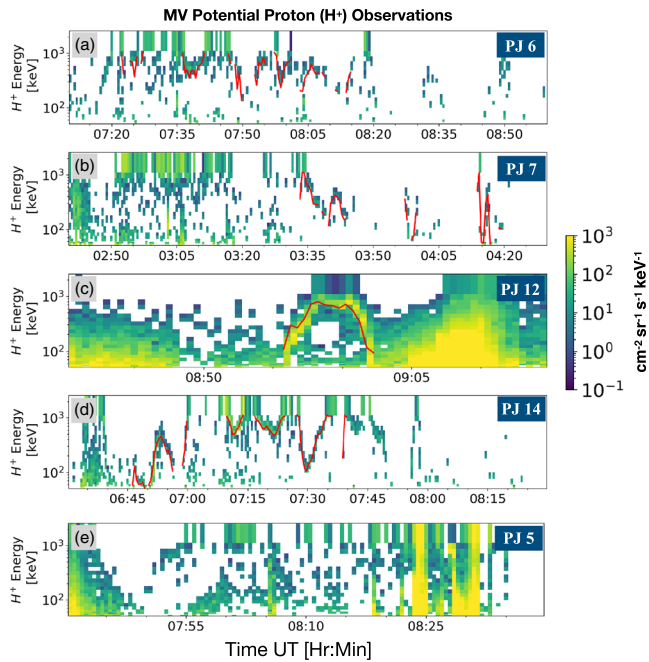


Figure 4. Proton (H^+) energy-time and intensity color coded spectrograms for five different MV potential signatures found in PJ6 (a), PJ7 (b), PJ12 (c), PJ14 (d), and PJ5 (e). We omit showing heavy ions here for clarity. Similar to Figure 2, the red curve represents the derived characteristic energy in keV. The first four candidates (a–d) represent the events used this study. The last candidate (e) still exhibits MV potential but is a nonideal candidate for charge state determination (see text).

combination of observed UV emissions and physical chemistry models that show the composition of the Io plasma torus is dominated by ($\sim 80\%$) O^+ and S^{++} in roughly equal amounts (e.g., see review paper by Bagenal & Dols, 2020). The results are also consistent with the higher energy ~ 100 keV/q ion measurements from the Cassini encounter with the distant ($\sim 200 R_J$) magnetosphere on the dusk flank (Allen et al., 2019). However, the results appear to differ slightly from the Clark et al. (2016) analysis of Galileo Energetic Particle Detector data which hinted that oxygen was more evenly distributed between O^+ and O^{++} . Even though the previous studies are all consistent with charge states being similar for $<MeV$ energies, that seems to change when comparing the results to those of Selesnick and Cohen (2009), which showed that very energetic heavy ions (≥ 5 MeV/nucleon) were dominantly fully stripped (or nearly fully) near Io. We present two ideas that may account for these differences in the literature: (1) The low-energy ($< tens$ of keV) ions are the source of the particles falling through the megavolt electric potentials and therefore these measurements best reflect the plasma distributions and (2) ion-neutral interactions are playing a role in redistributing the heavy ion charge states in Jupiter's inner-to-middle magnetosphere. These two ideas are not necessarily mutually exclusive either.

The first idea is based on the observations that the partial density ratios within the acceleration region are in better agreement with the lower-energy plasma (< 40 keV/Q) observations (Kim et al., 2020) rather than JEDI results of the conjugate magnetic equator (see Figure 6). This straightforward interpretation means that Juno/JEDI is effectively sounding the plasma that resides in the distant magnetosphere, and therefore, one would expect a general agreement. For the same reasons, it also means that the charge state distributions presented here may not be representative of the trapped populations of energetic charged particles, which may have been accelerated very differently to high energies.

The second idea is based on the apparent evolution of ions to higher charge states with decreasing radial distance (Clark, Mauk, et al., 2016; Selesnick & Cohen, 2009). We hypothesize that at ion energies $> hundreds$ of keV, the higher charge states are favored because the charge stripping cross sections become more important. Clark, Mauk, et al. (2016) first discussed this scenario and showed that indeed, the σ_{12} (charge stripping) cross section is comparable to σ_{10} (charge exchange) for oxygen at ~ 500 keV and dominant at energies > 1 MeV. The lack of evidence of predominately high-charge state oxygen in these observations (which map to equatorial distances $> 60 R_J$) as well as the ~ 100 keV/q ions near the magnetopause (Allen et al., 2019) may provide circumstantial evidence that the trans-Europa neutral cloud (Kollmann et al., 2016; Lagg et al., 2003; Mauk et al., 2003; Nénon & André, 2019) starts to redistribute the singly charged oxygen to higher charge states and eventually becomes fully stripped near Io. The dependence on radial distance arises because the density of neutrals increases (Bagenal & Dols, 2020) as well as the ion characteristic energies and ion residence times (Mauk et al., 2004) with decreasing radial distance.

5.2. Possible Relationship to Soft X-Ray Polar Emissions

Soft X-ray auroral emissions ($\lesssim 3$ keV) from Jupiter's polar regions have been studied for the better part of four decades with observations from Earth-based observatories (e.g., Bhardwaj & Gladstone, 2000; Dunn et al., 2017; Gladstone et al., 2002; Jackman et al., 2018; Metzger et al., 1983; Waite et al., 1994). From these observations, two leading hypotheses have emerged for generation of soft X-rays, namely, via (1) precipitating energetic oxygen and sulfur ions (e.g., Metzger et al., 1983; Waite et al., 1994) or (2) the precipitation of high-charge state solar wind oxygen (O^{6+}) into Jupiter's polar region (e.g., Branduardi-Raymont et al., 2004). While hard X-ray (> 2 keV) electron bremsstrahlung emission is produced along the UV aurora main emission (Branduardi-Raymont et al., 2004, 2007), other studies, such as Gladstone et al. (2002), demonstrate that

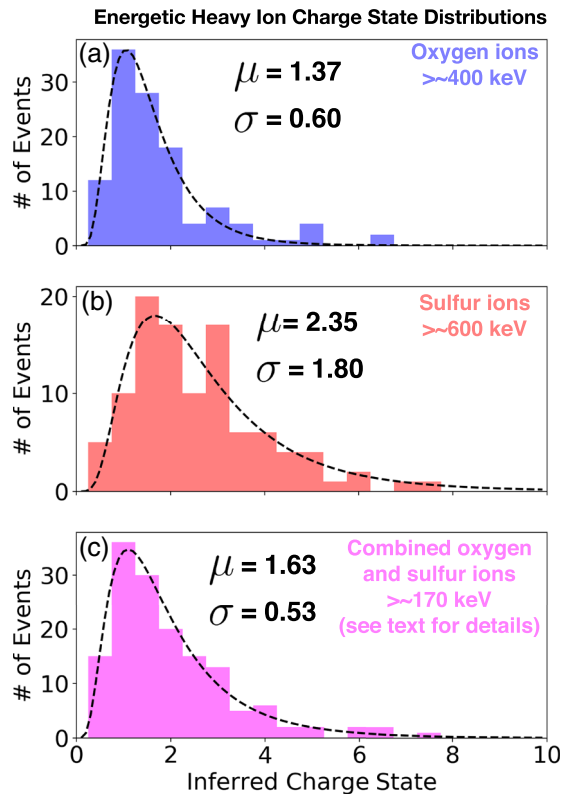


Figure 5. Frequency distributions depicting the oxygen (a), sulfur (b), and combined O and S (c) to proton characteristic energy ratios. Black dashed curves correspond to log-normal fits with the associated parameters μ and σ labeled in each panel (see text for details).

electron bremsstrahlung cannot account for the energetics associated with the soft X-rays and neither are the heavy ion intensities beyond $\sim 30 R_J$ capable of producing the observed X-ray brightness. These shortcomings lead the authors to postulate that a process has yet to be identified that can account for all the details. More recent observations from Chandra, XMM-Newton, and supporting ion-chemistry models of Jupiter's upper atmosphere appear to favor the scenario of precipitating energetic magnetospheric ions but have also revealed complexities arising from nonconjugate processes (Dunn et al., 2017) and possible correlations with solar wind activity (Dunn et al., 2016; Kimura et al., 2016). Spectral information from Chandra and XMM-Newton can also be used to measure the sulfur to oxygen ion ratios. Dunn et al. (2020) found that the S^{n+}/O^{n+} ratio is ~ 0.4 to 1.3, or equivalently, the O/S ratio is ~ 0.75 to 2.5.

We established in the previous section that the energetic heavy ions associated with the MV potentials appear to be predominately iogenic O^+ and S^{++} , with partial density ratios of $O^{n+}/S^{n+} \sim 1$ and greater. The ratios agree surprisingly well with the O^{n+}/S^{n+} abundance ratios presented by Dunn et al. (2020). Additionally, Mauk et al. (2020) reviewed the polar cap auroral region and showed that MV potentials are observable for $\sim 80\%$ of the polar cap crossings and occur over a substantial fraction of the polar cap area. These sources of observational evidence stacked together support the hypothesis that Jupiter's soft X-ray emissions are sourced from magnetospheric ions originating in Jupiter's outer magnetosphere. Although we only focus on a subset of polar cap crossings in our charge state analysis, we have no reason to believe that the other crossings are in any way fundamentally different. In fact, we show an alternative method in Appendix A that uses data from PJs 1–14, and it supports our claim.

If O^{6+} were present in similar quantities, then our method would be capable of distinguishing such high charge state from O^+ or O^{++} . The only possible issue with this hypothesis is that the magnetic field strength near Jupiter is orders of magnitude higher than in the outer magnetosphere, meaning that the loss cone for heavy ions to reach the planet is practically vanishingly small, unless other processes, such as large potentials, exist on significant parts of these field lines.

Another consequence from the results presented in section 4 and the Mauk et al. (2020) overview suggests that precipitation is (nearly) always accompanied by the presence of quasi-static electric potentials, suggesting that precipitation of >100 – 300 keV/nucleon heavy ions via pitch angle scattering (e.g., Gehrels & Stone, 1983; Horanyi et al., 1988) may not be the only or primary mechanism. We note that Haggerty et al. (2017) was the first to show evidence of heavy ion precipitation in the polar region from JEDI observations. At the time, pitch angle scattering was suggested as a potential mechanism, but a reanalysis of the PJ1 event has shown that electric potentials are indeed present (Mauk et al., 2020). We believe this is a significant observation that must be reconciled with the future interpretations of X-ray sources, namely, how do these large-scale electric potentials develop and what is the role of pitch angle scattering to fill the loss cone with energetic ions? Regarding the former, Bunce et al. (2004) discussed the possibility of pulsed reconnection in the Jovian cusp generating potential drops on the order of several MV. Interestingly, these values are commensurate with our observations of the heavy ion characteristic energies; however, we show here and in Mauk et al. (2020) that these megavolt structures occur over a large swath of the polar cap region, and therefore, it is unclear how these relate to a cusp-like process, which is more localized.

Finally, Mauk et al. (2020) hypothesized that the observations of MV potentials may be organized by an altitude effect, that is, the spacecraft needs to be below $\sim 2.5 R_J$ to observe the potentials. This is important to note because the Juno spacecraft has not spent much time within the northern X-ray hot spot region below these altitudes, although we know X-ray emissions are generated over a large range of System III latitudes

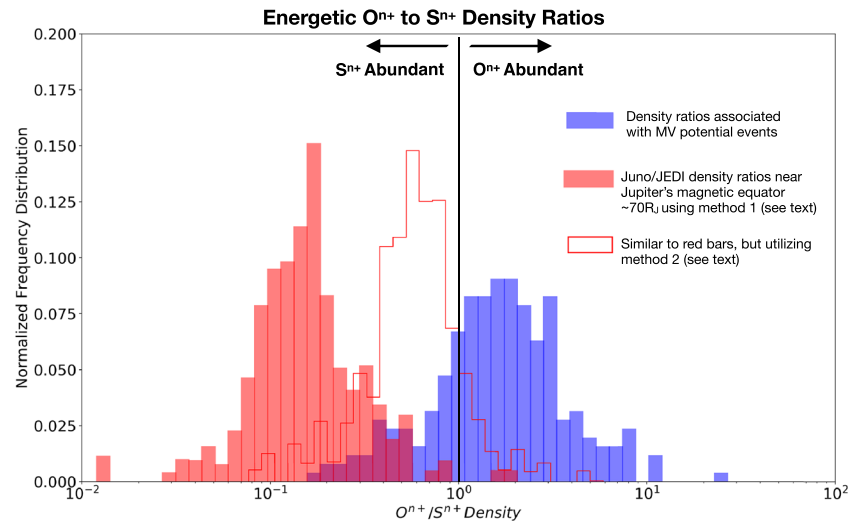


Figure 6. Normalized frequency distributions of the O^{n+} to S^{n+} density ratios for three different cases: (1) events associated with the MV potentials used in our charge state analysis (blue bars), (2) events associated with Jupiter's magnetic equator that include overlapping O^{n+} and S^{n+} energy channels (red bars), and (3) the events from all O^{n+} and S^{n+} energy channels (red step trace).

and longitudes poleward of the main aurora (Gladstone et al., 2002). We predict that future excursions of this region by Juno (in a potential extended mission) should reveal the presence of MV potentials and heavy ion properties consistent with what is presented. We bring attention to this point to demonstrate that the results here have their limitations and do not necessarily preclude other theories for soft X-ray generation.

6. Summary

In this contribution, we have analyzed energetic heavy ions accelerated by megavolt electric potentials and have inferred their charge state. Below is a summary of our findings and discussion points:

1. The primary charge states in Jupiter's low-altitude polar cap region appears to be O^+ and S^{++} , with smaller contributions from O^{++} and S^+ and S^{+++} . This suggests that the plasma is iogenic in origin.
2. The partial mass density ratios of O^{n+} to S^{n+} associated with MV potentials suggest that their ion composition is mostly oxygen abundant with a large fraction of the events consisting of $O^{n+}/S^{n+} > 1$.
3. The mass density ratios appear to agree well with ion plasma measurements (Kim et al., 2020) and O:S abundance ratios inferred from X-ray spectral observations (Dunn et al., 2020).
4. We propose that ion-neutral interactions are playing a role in redistributing the energetic (>hundreds of keV) heavy ion charge states near the trans-Europa cloud and inward. This idea reconciles the observational differences that show the charge states of energetic oxygen are primarily O^+ at large distances (this work and Allen et al., 2019), a more even mixture of O^+ and O^{++} is found near the neutral cloud (Clark, Mauk, et al., 2016), and a maximum charge state value of O^{8+} is found near Io (Selesnick & Cohen, 2009).
5. The recent overview from Mauk et al. (2020) showing that megavolt potentials span most of the polar cap area (see our Figure 1, magenta curves) and the analysis of the associated heavy ions in this paper, we believe this supports the hypothesis of soft X-ray emissions that are sourced by precipitating energetic heavy ions. In addition, we also suggest that MV potentials are an important acceleration mechanism to consider in addition to pitch angle scattering of energetic ions in Jupiter's outer magnetosphere.

Appendix A: Ion Energy Correlation Technique to Infer Charge State

We adopt an analysis technique that was first used by Mitchell et al. (2018) to explore the charge-dependent adiabatic energization of ions in Earth's magnetosphere. It should be noted that the instrument used by Mitchell et al. (2018) is very similar to the Juno/JEDI instrument, and both were developed at the same institution (Clark, Cohen, et al., 2016; Mauk et al., 2017; Mitchell et al., 2013). Therefore, to zeroth order, the two instruments have comparable responses to protons and heavy ions and over a similar energy range. The

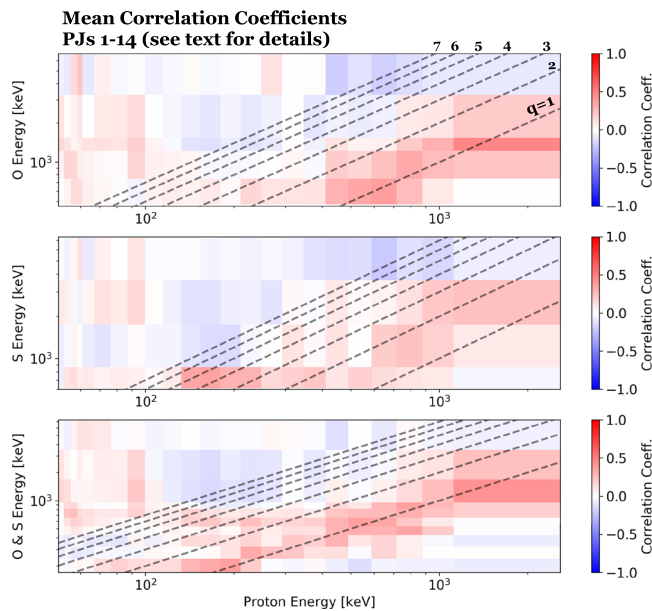


Figure A1. Ion energy-time correlation matrices for oxygen ions (top panel), sulfur ions (middle panel), and combined oxygen and sulfur ions (bottom panel). The color coded pixels represent the Pearson correlation coefficient, and the dashed lines correspond to charge state slopes of 1 through 7 (see top panel for labeling).

technique developed by Mitchell et al. (2018) relies on the time series correlations between different species and energy channels. Using the protons as the fiducial since they have a charge state equal to one, the heavy ion intensities are then correlated to the proton intensities. If the acceleration mechanism is truly charge dependent, the governing assumption in this analysis technique, then the heavy ion energy channels that correlate best to the protons can be used to infer the charge state. For example, Mitchell et al. (2018) found that He energy channels at twice the energy of the proton energy channels returned the highest correlations. Therefore, since $q_{\text{He}}E_{\text{He}} = 2 \times q_{\text{H}^+}E_{\text{H}^+} \rightarrow q_{\text{He}} = 2$, since $q_{\text{H}^+} = 1$. This is expected because solar wind alpha particles may be the primary source of helium in Earth's magnetosphere.

This technique is applied to Juno/JEDI observations of quasi-static electric potentials in Jupiter's polar cap region spanning PJs 1–14. Figure A1 shows the time series correlation maps of the three heavy ion channels: >400 keV oxygen (top panel), >600 keV sulfur (middle panel), and >170 keV oxygen and sulfur (bottom panel). The dashed lines overlaid represent the various charge state slopes associated with $q = 1, 2, 3$, and so forth. (see top panel for labeling). Evident in Figure A1 are the clustering of moderate positive correlation values (~ 0.3 to >0.5) around the $q = 1$ slope for oxygen, $q = 2$ slope for sulfur, and $q = 1$ slopes for the combined oxygen and sulfur channels. These results therefore show good agreement with our method outlined in section 3 and provide an independent confirmation. The

fact that the combined oxygen and sulfur channels cluster around $q = 1$, which is found in the pure oxygen channel, also indicates that the lower-energy heavy ion channels are dominated by oxygen.

We chose to not base our conclusions purely on this analysis technique because of the limitations outnumber those with the characteristic energy approach presented in section 3. For example, this method is susceptible to penetrating radiation, which is evident by the apparent correlation of all heavy ion energies with low-energy protons. The lower-energy protons have longer times-of-flight, and therefore, the timing window is more susceptible to false coincidences generated by penetrating radiation, which is likely due to the presence of $> \text{MeV}$ electrons (Mauk et al., 2020; Paranicas et al., 2018). Our characteristic energy approach is less sensitive to backgrounds due to the peaked-energy distributions being well defined (see Figure 4). Second, the energy-correlation method is also prone to statistical counting fluctuations as evident by the weak negative correlations found throughout the correlation matrix. One could filter these out, but we found it was not necessary and did not impact the results. These limitations appear to be environment specific because they are not shared with Mitchell et al. (2018) study that used this technique for Earth's equatorial magnetosphere.

Data Availability Statement

The data presented here are available from the Planetary Plasma Interactions Node of NASA's Planetary Data System (<https://pds-ppi.igpp.ucla.edu/>). ACSII files associated with the figures presented here and this paper is accessible on Zenodo, an open-access repository (<http://doi.org/10.5281/zenodo.3890179>), and at the Juno Science Operations Center (archive link is under construction).

References

Allen, R. C., Mitchell, D. G., Paranicas, C. P., Hamilton, D. C., Clark, G., Rymer, A. M., et al. (2018). Internal versus external sources of plasma at Saturn: Overview from Magnetospheric imaging investigation/charge-energy-mass spectrometer data. *Journal of Geophysical Research: Space Physics*, 123, 4712–4727. <https://doi.org/10.1029/2018JA025262>

Allen, R. C., Paranicas, C. P., Bagenal, F., Vines, S. K., Hamilton, D. C., Allegrini, F., et al. (2019). Energetic oxygen and sulfur charge states in the outer Jovian magnetosphere: Insights from the Cassini Jupiter flyby. *Geophysical Research Letters*, 46, 11709–11717. <https://doi.org/10.1029/2019GL085185>

Acknowledgments

We are thankful to the institutions and personnel that made the Juno mission and the JEDI instrument a success. We are also grateful to JHU/APL's Lawrence Brown and James Peachy for their roles in developing the core of the data display software. This work has been funded by NASA's New Frontiers Program for Juno via a subcontract with the Southwest Research Institute in San Antonio, Texas.

- Bagenal, F., & Delamere, P. A. (2011). Flow of mass and energy in the magnetospheres of Jupiter and Saturn. *Journal of Geophysical Research*, *116*, A05209. <https://doi.org/10.1029/2010JA016294>
- Bagenal, F., Dols, V. (2020). The space environment of Io and Europa. *Journal of Geophysical Research: Space Physics*, *125* <https://doi.org/10.1029/2019JA027485>
- Bagenal, F., Dougherty, L. P., Bodisch, K. M., Richardson, J. D., & Belcher, J. M. (2017). Survey of Voyager plasma science ions at Jupiter: 1 Analysis method. *Journal of Geophysical Research: Space Physics*, *122*, 8241–8256. <https://doi.org/10.1002/2016JA023797>
- Bhardwaj, A., & Gladstone, G. R. (2000). Auroral emissions of the giant planets. *Reviews of Geophysics*, *38*, 295–353.
- Bolton, S. J., Adriani, A., Adumitroaie, V., Allison, M., Anderson, J., Atreya, S., et al. (2017). Jupiter's interior and deep atmosphere: The initial pole-to-pole passes with the Juno spacecraft. *Science*, *356*(6340), 821–825. <https://doi.org/10.1126/science.aal2108>
- Branduardi-Raymont, G., Bhardwaj, A., Elsner, R. F., Gladstone, G. R., Ramsay, G., Rodriguez, P., et al. (2007). A study of Jupiter's aurorae with XMM-Newton. *A&A*, *463*(2), 761–774. Retrieved from. <https://doi.org/10.1051/0004-6361:20066406>
- Branduardi-Raymont, G., Elsner, R. F., Gladstone, G. R., Ramsay, G., Rodriguez, P., Soria, R., & Waite, J. H. (2004). First observation of Jupiter by XMM-Newton. *A&A*, *424*(1), 331–337. Retrieved from. <https://doi.org/10.1051/0004-6361:20041149>
- Bunce, E. J., Cowley, S. W. H., & Yeoman, T. K. (2004). Jovian cusp processes: Implications for the polar aurora. *Journal of Geophysical Research*, *109*, A09S13. <https://doi.org/10.1029/2003JA010280>
- Carlson, C. W., McFadden, J. P., Ergun, R. E., Temerin, M., Peria, W., Mozer, F. S., et al. (1998). FAST observations in the downward auroral current region: Energetic upgoing electron beams, parallel potential drops, and ion heating. *Geophysical Research Letters*, *25*(12), 2017–2020. <https://doi.org/10.1029/98GL00851>
- Clark, G., Cohen, I., Westlake, J. H., Andrews, G. B., Brandt, P., Gold, R. E., et al. (2016). The “Puck” energetic charged particle detector: Design, heritage, and advancements. *Journal of Geophysical Research: Space Physics: Space Physics*, *121*, 7900–7913. <https://doi.org/10.1002/2016JA022579>
- Clark, G., Mauk, B. H., Haggerty, D., Paranicas, C., Kollmann, P., Rymer, A., et al. (2017). Energetic particle signatures of magnetic field-aligned potentials over Jupiter's polar regions. *Geophysical Research Letters*, *44*, 8703–8711. <https://doi.org/10.1002/2017GL074366>
- Clark, G., Mauk, B. H., Paranicas, C., Kollmann, P., & Smith, H. T. (2016). Charge states of energetic oxygen and sulfur ions in Jupiter's magnetosphere. *Journal of Geophysical Research: Space Physics*, *121*, 2264–2273. <https://doi.org/10.1002/2015JA022257>
- Clark, G., Tao, C., Mauk, B. H., Nichols, J., Saur, J., Bunce, E. J., et al. (2018). Precipitating electron energy flux and characteristic energies in Jupiter's main auroral region as measured by Juno/JEDI. *Journal of Geophysical Research: Space Physics*, *123*, 7554–7567. <https://doi.org/10.1029/2018JA025639>
- Cohen, C. M. S., Stone, E. C., & Selesnick, R. S. (2001). Energetic ion observations in the middle Jovian magnetosphere. *Journal of Geophysical Research*, *106*(A12), 29871–29881. <https://doi.org/10.1029/2001JA000008>
- Connerney, J. E. P., Açuna, M. H., & Ness, N. F. (1981). Modeling the Jovian current sheet and inner magnetosphere. *Journal of Geophysical Research*, *86*(A10), 8370–8384. <https://doi.org/10.1029/JA086iA10p08370>
- Connerney, J. E. P., Adriani, A., Allegrini, F., Bagenal, F., Bolton, S. J., Bonfond, B., et al. (2017). Jupiter's magnetosphere and aurorae observed by the Juno spacecraft during its first polar orbits. *Science*, *356*(6340), 826–832. <https://doi.org/10.1126/science.aam5928>
- Connerney, J. E. P., Bann, M., Bjarno, J. B., Denver, T., Espley, J., Jorgensen, J. L., et al. (2017). The Juno magnetic field investigation. *Space Science Reviews*, *213*(1-4), 39–138. <https://doi.org/10.1007/s11214-017-0334-z>
- Connerney, J. E. P., Kotsiaros, S., Oliverson, R. J., Espley, J. R., Joergensen, J. L., Joergensen, P. S., et al. (2018). A new model of Jupiter's magnetic field from Juno's first nine orbits. *Geophysical Research Letters*, *45*, 2590–2596. <https://doi.org/10.1002/2018GL077312>
- Cravens, T. E., Waite, J. H., Gombosi, T. I., Lugaz, N., Gladstone, G. R., Mauk, B. H., & MacDowall, R. J. (2003). Implications of Jovian X-ray emission for magnetosphere-ionosphere coupling. *Journal of Geophysical Research*, *108*(A12), 1465. <https://doi.org/10.1029/2003JA010050>
- Delamere, P. A., Bagenal, F., Dols, V., & Ray, L. (2007). Saturn's neutral torus vs. Jupiter's plasma torus. *Geophysical Research Letters*, *34*, L09105. <https://doi.org/10.1029/2007GL029437>
- Dunn, W. R., Branduardi-Raymont, G., Carter-Cortez, V., Campbell, A., Elsner, R., Ness, J.-U., et al. (2020). Jupiter's X-rays 2007 Part 1: Jupiter's X-ray Emission During Solar Minimum. *Journal of Geophysical Research: Space Physics*, e2019JA027219. <https://doi.org/10.1029/2019ja027219>
- Dunn, W. R., Branduardi-Raymont, G., Elsner, R. F., Vogt, M. F., Lamy, L., Ford, P. G., et al. (2016). The impact of an ICME on the Jovian X-ray aurora. *Journal of Geophysical Research: Space Physics*, *121*, 2274–2307. <https://doi.org/10.1002/2015JA021888>
- Dunn, W. R., Branduardi-Raymont, G., Ray, L. C., Jackman, C. M., Kraft, R. P., Elsner, R. F., et al. (2017). The independent pulsations of Jupiter's northern and southern X-ray auroras. *Nature Astronomy*, *1*(11), 758–764. <https://doi.org/10.1038/s41550-017-0262-6>
- Elsner, R. F., Gladstone, G. R., Waite, J. H., Crary, F. J., Howell, R. R., Johnson, R. E., et al. (2002). Discovery of soft X-ray emission from Io, Europa, and the Io plasma torus. *The Astrophysical Journal*, *572*(2), 1077–1082. <https://doi.org/10.1086/340434>
- Ergun, R. E., Carlson, C. W., McFadden, J. P., Mozer, F. S., Delory, G. T., Peria, W., et al. (1998). FAST satellite observations of electric field structures in the auroral zone. *FAST satellite observations of electric field structures in the auroral zone*, *25*(12), 2025–2028. <https://doi.org/10.1029/98GL00635>
- Garrard, T. L., Stone, E. C., & Murphy, N. (1996). Effects of absorption by Io on composition of energetic heavy ions. *Science*, *274*(5286), 393–394. <https://doi.org/10.1126/science.274.5286.393>
- Gehrels, N., & Stone, E. C. (1983). Energetic oxygen and sulfur ions in the Jovian magnetosphere and their contribution to the auroral excitation. *Journal of Geophysical Research*, *88*(A7), 5537–5550. <https://doi.org/10.1029/JA088iA07p05537>
- Gladstone, G. R., Waite, J. H. Jr., Grodent, D., Lewis, W. S., Crary, F. J., Elsner, R. F., et al. (2002). A pulsating auroral X-ray hot spot on Jupiter. *Nature*, *415*(6875), 1000–1003. <https://doi.org/10.1038/4151000a>
- Haggerty, D. K., Mauk, B. H., Paranicas, C. P., Clark, G., Kollmann, P., Rymer, A. M., et al. (2017). Juno/JEDI observations of 0.01 to >10 MeV energetic ions in the Jovian auroral regions: Anticipating a source for polar X-ray emission. *Geophysical Research Letters*, *44*, 6476–6482. <https://doi.org/10.1002/2017GL072866>
- Hansen, C., Shemansky, D., & Hendrix, A. (2005). Cassini UVIS observations of Europa's oxygen atmosphere and torus. *Icarus*, *176*(2), 305–315. <https://doi.org/10.1016/j.icarus.2005.02.007>
- Horanyi, M., Cravens, T. E., & Waite, J. H. (1988). The precipitation of energetic heavy ions into the upper atmosphere of Jupiter. *Journal of Geophysical Research*, *93*(A7), 7251–7271. <https://doi.org/10.1029/JA093iA07p07251>
- Houston, S. J., Ozak, N., Young, J., Cravens, T. E., & Schultz, D. R. (2018). Jovian auroral ion precipitation: Field-aligned currents and ultraviolet emissions. *Journal of Geophysical Research: Space Physics*, *123*, 2257–2273. <https://doi.org/10.1002/2017JA024872>

- Jackman, C. M., Knigge, C., Altamirano, D., Gladstone, R., Dunn, W., Elsner, R., et al. (2018). Assessing quasi-periodicities in Jovian X-ray emissions: Techniques and heritage survey. *Journal of Geophysical Research: Space Physics*, *123*, 9204–9221. <https://doi.org/10.1029/2018JA025490>
- Kim, T. K., Ebert, R. W., Valek, P. W., Allegrini, F., McComas, D. J., Bagenal, F., et al. (2020). Method to derive ion properties from Juno JADE including abundance estimates for O^+ and S^{2+} . *Journal of Geophysical Research: Space Physics*, *125*. <https://doi.org/10.1029/2018JA026169>
- Kimura, T., Kraft, R. P., Elsner, R. F., Branduardi-Raymont, G., Gladstone, G. R., Tao, C., et al. (2016). Jupiter's X-ray and EUV auroras monitored by Chandra, XMM-Newton, and Hisaki satellite. *Journal of Geophysical Research: Space Physics*, *121*, 2308–2320. <https://doi.org/10.1002/2015JA021893>
- Kivelson, M. G., Bagenal, F., Kurth, W. S., Neubauer, F. M., Paranicas, C., & Saur, J. (2004). The Io neutral clouds and plasma torus. In F. Bagenal, T. E. Dowling, & W. B. McKinnon (Eds.), *Jupiter: The planet, satellites and magnetosphere* (pp. 561–591). New York: Cambridge University Press.
- Khurana, K. K., Kivelson, M. G., Vasylinuas, V. M., Krupp, N., Woch, J., Lagg, A., et al. (2004). The Configuration of Jupiter's Magnetosphere. In F. Bagenal, T. E. Dowling, & W. B. McKinnon (Eds.), *Jupiter: The planet, satellites and magnetosphere* (pp. 561–591). New York: Cambridge University Press.
- Kollmann, P., Paranicas, C., Clark, G., Roussos, E., Lagg, A., & Krupp, N. (2016). The vertical thickness of Jupiter's Europa torus from charged particle measurements. *Geophysical Research Letters*, *43*, 9425–9433. <https://doi.org/10.1002/2016GL070326>
- Kronberg, E. A., Grigorenko, E. E., Malykhin, A., Kozak, L., Petrenko, B., Vogt, M. F., et al. (2019). Acceleration of ions in Jovian plasmoids: Does turbulence play a role? *Journal of Geophysical Research: Space Physics*, *124*, 5056–5069. <https://doi.org/10.1029/2019JA026553>
- Krupp, N., Woch, J., Lagg, A., Livi, S., Mitchell, D. G., Krimigis, S. M., et al. (2004). Energetic particle observations in the vicinity of Jupiter: Cassini MIMI/LEMMS results. *Journal of Geophysical Research*, *109*, A09S10. <https://doi.org/10.1029/2003JA010111>
- Lagg, A., Krupp, N., Woch, J., & Williams, D. J. (2003). In-situ observations of a neutral gas torus at Europa. *Geophysical Research Letters*, *30*(11), 1556. <https://doi.org/10.1029/2003GL01721>
- Lin, C. S., & Hoffman, R. A. (1982). Observations of inverted-V electron precipitation. *Space Science Reviews*, *33*(4), 415–457. <https://doi.org/10.1007/BF00212420>
- Mitchell, D. G., Lanzerotti, L. J., Kim, C. K., Stokes, M., Ho, G., Cooper, S., et al. (2013). Radiation Belt Storm Probes Ion Composition Experiment (RBSPICE). In N. Fox & J. L. Burch *The Van Allen Probes Mission* (pp. 263–308). Springer, Boston, MA. https://doi.org/10.1007/978-1-4899-7433-4_8
- Mauk, B. H., Clark, G., Gladstone, G. R., Kotsiaros, S., Adriani, A., Allegrini, F., et al. (2020). Energetic particles and acceleration regions over Jupiter's polar cap and main aurora; a broad overview. *Journal of Geophysical Research: Space Physics*, *125*. <https://doi.org/10.1029/2019JA027699>
- Mauk, B. H., Cohen, I. J., Haggerty, D. K., Hospodarsky, G. B., Connerney, J. E. P., Anderson, B. J., et al. (2019). Investigation of mass-/charge-dependent escape of energetic ions across the magnetopauses of Earth and Jupiter. *Journal of Geophysical Research: Space Physics*, *124*(7), 5539–5567. <https://doi.org/10.1029/2019JA026626>
- Mauk, B. H., Haggerty, D. K., Jaskulek, S. E., Schlemm, C. E., Brown, L. E., Cooper, S. A., et al. (2017). The Jupiter Energetic Particle Detector Instrument (JEDI) Investigation for the Juno Mission. *Space Science Reviews*, *213*(1–4), 289–346. <https://doi.org/10.1007/s11214-013-0025-3>
- Mauk, B. H., Mitchell, D. G., Krimigis, S. M., Roelof, E. C., & Paranicas, C. P. (2003). Energetic neutral atoms from a trans-Europa gas torus at Jupiter. *Nature*, *421*(6926), 920–922. <https://doi.org/10.1038/nature01431>
- Mauk, B. H., Mitchell, D. G., McEntire, R. W., Paranicas, C. P., Roelof, E. C., Williams, D. J., et al. (2004). Energetic ion characteristics and neutral gas interactions in Jupiter's magnetosphere. *Journal of Geophysical Research*, *109*, A09S12. <https://doi.org/10.1029/2003JA010270>
- Metzger, A. E., Gilman, D. A., Luthey, J. L., Hurley, K. C., Schnopper, H. W., Seward, F. D., & Sullivan, J. D. (1983). The detection of X-rays from Jupiter. *Journal of Geophysical Research*, *88*(A10), 7731–7741. <https://doi.org/10.1029/JA088iA10p07731>
- Mitchell, D. G., Gkioulidou, M., & Ukhorskiy, A. Y. (2018). Energetic ion injections inside geosynchronous orbit: Convection- and drift-dominated, charge-dependent adiabatic energization ($W = qEd$). *Journal of Geophysical Research: Space Physics*, *123*, 6360–6382. <https://doi.org/10.1029/2018JA025556>
- Nénon, Q., & André, N. (2019). Evidence of Europa neutral gas torii from energetic sulfur ion measurements. *Geophysical Research Letters*, *46*, 3599–3606. <https://doi.org/10.1029/2019GL082200>
- Ozak, N., Schultz, D. R., Cravens, T. E., Kharchenko, V., & Hui, Y.-W. (2010). Auroral X-ray emission at Jupiter: Depth effects. *Journal of Geophysical Research*, *115*, A11306. <https://doi.org/10.1029/2010JA015635>
- Paranicas, C., Cooper, J. F., Garrett, H. B., Johnson, R. E., & Sturmer, S. J. (2009). "Europa's radiation environment and its effects on the surface." *Europa*. Ed. R. T. Pappalardo, W. B. McKinnon, and K. Khurana, 529–44. Print.
- Paranicas, C., Mauk, B. H., Haggerty, D. K., Clark, G., Kollmann, P., Rymer, A. M., et al. (2018). Intervals of intense energetic electron beams over Jupiter's poles. *Journal of Geophysical Research: Space Physics*, *123*(3), 1989–1999. <https://doi.org/10.1002/2017JA025106>
- Schneider, N. M., & Bagenal, F. (2007). Io's neutral clouds, plasma torus, magnetospheric interaction. In *Io After Galileo*. Springer Praxis Books (pp. 265–286). Springer, Berlin, Heidelberg. https://doi.org/10.1007/978-3-540-48841-5_11
- Selesnick, R. S., & Cohen, C. M. S. (2009). Charge states of energetic ions in Jupiter's radiation belt inferred from absorption microsignatures of Io. *Journal of Geophysical Research*, *114*, A01207. <https://doi.org/10.1029/2008JA013722>
- Smith, H. T., Mitchell, D. G., Johnson, R. E., Mauk, B. H., & Smith, J. E. (2019). Europa neutral torus confirmation and characterization based on observations and modeling. *The Astrophysical Journal*, *871*(1), 69. <https://doi.org/10.3847/1538-4357/aaed38>
- Szalay, J. R., Allegrini, F., Bagenal, F., Bolton, S., Clark, G., Connerney, J. E. P., et al. (2017). Plasma measurements in the Jovian polar region with Juno/JADE. *Geophysical Research Letters*, *44*, 7122–7130. <https://doi.org/10.1002/2017GL072837>
- Thomas, N., Bagenal, F., Hill, T. W., & Wilson, J. K. (2004). The Io neutral clouds and plasma torus. In F. Bagenal, T. E. Dowling, & W. B. McKinnon (Eds.), *Jupiter: The planet, satellites and magnetosphere* (pp. 561–591). New York: Cambridge University Press.
- Waite, J. H., Bagenal, F., Seward, F., Na, C., Gladstone, G. R., Cravens, T. E., et al. (1994). ROSAT observations of the Jupiter aurora. *Journal of Geophysical Research*, *99*(A8), 14,799–14,809. <https://doi.org/10.1029/94JA01005>